RSC Advances

PAPER

View Article Online
View Journal | View Issue

Cite this: *RSC Adv.*, 2022, **12**, 9342

Tuning luminescence of the fluorescent molecule 2-(2-hydroxyphenyl)-1*H*-benzimidazole *via* zeolitic imidazolate framework-8

Yuyi Zhang,[a] Wei Zhang,[a] Yajie Bian,[a] Yiting Liu,[a] Xiaolei Zhang, *[ab] Mengdi Chen, *[a] Bingwen Hu [a] and Qingyuan Jin*[ac]

Received 30th December 2021
Accepted 18th March 2022

DOI: 10.1039/d1ra09446g

rsc.li/rsc-advances

Zeolitic imidazolate framework-8 (ZIF-8) is one of the most promising metal–organic frameworks because of its excellent high porosity, stability and geometrically well-defined structure. However, the application of ZIF-8 in the field of fluorescent molecular sensing has not been intensively explored. Our work demonstrates the versatility of ZIF-8 as a carrier material, which can be used for small molecule [2-(2-hydroxyphenyl)-1*H*-benzimidazole (HPBI)] capture and fluorescence enhancement. ZIF-8 displays luminescent behavior changes when combined with HPBI, as the emission peaks of ZIF-8 and HPBI are located in the same range for resonance enhancement of fluorescence. The results of the experiment indicate that the fluorescence enhancement effect will change in the presence of different concentrations of HPBI. We propose that the pore structure of ZIF-8 could provide an opportunity for the adsorption of HPBI molecules, and eventually the adsorption would saturate. The high porosity of ZIF-8 provides the path to HPBI aggregation or entrance into the ZIF-8 internal structure. Our results suggest that ZIF-8 may offer great promise for molecular fluorescence sensing.

1 Introduction

Metal–organic frameworks (MOFs) are highly-porous hybrid materials built with metal centers and organic ligands, different from the conventionally used microporous and mesoporous materials (*e.g.* activated carbons, silicas, and zeolites). These metal–organic structures exhibit the potential for more flexible rational design, and possess open framework structures with inherently high microporosity. The molecular characteristics allow controlling the size and the surface functionalization of the organic linkers and pores.[1–3] The unique structure of MOFs has enabled them to be useful in various applications, including gas storage, catalysis, molecular recognition, separation, luminescent sensing, and many others.[4–11] For sensing molecular systems, the inner guest molecule and the outer host molecule are generally combined. To serve as a useful sensor, MOFs with structural rigidity, high porosity, and geometrically well-defined structures are capable of detecting specific molecules.[12–17] When the laser excites MOFs binding to guest molecules, they can respond to the luminescence changes, with the charge or energy transfer between MOFs and guest molecules, and the tunability of MOFs sorption properties provides a high degree of molecular specificity.[18–21] There already have been studies of how molecular sieving can be used for size selective sensing in luminescent $Zn_3(BTC)_2$ (BTC= 1,3,5-benzenetricarboxylate), which can coordinate water and other molecules without destructing the framework.[22,23] Meanwhile, a variety of transition metals such as Cd(II) and Zn(II) have been used in cases where linker-based or linker-metal luminescence is observed, many MOFs contain conjugated ligands that absorb in the visible or UV region. Depending on the metal's electronic configuration, relative metal and linker orbital energies, the metal ion can have varying degrees of influence on the emission.[23–25] Several transition metal–organic frameworks used for molecular sensing have also been reported, such as the sensing of ethylamine in Zn(BDC) with fluorescence detection,[26] the detection of both DNT and DMNB with a highly luminescent microporous metal–organic framework $[Zn_2(bpdc)_2(bpee)]$ (bpdc = 4,4′-biphenyldicarboxylate; bpee = 1,2-bipyridylethene),[27] and the selectivity detection of high explosives using a highly luminescent three-dimensional microporous metal–organic framework $[Zn_2(oba)_2(bpy)]\cdot DMA$.[28]

Imidazole nitrogen sites within porous Zeolitic Imidazolate Frameworks (ZIFs) are expected to play roles in the recognition of molecules. Zeolitic imidazolate framework-8 (ZIF-8) is a typical MOF, consisting of M-IM-M units where M and IM respectively represent the metal cations (*e.g.* Zn(II)) and the

[a]*State Key Laboratory of Precision Spectroscopy, Shanghai Key Laboratory of Magnetic Resonance, School of Physics and Electronic Science, East China Normal University, Shanghai 200062, China. E-mail: xlzhang@admin.ecnu.edu.cn; mdchen@lps.ecnu.edu.cn; qyjin@phy.ecnu.edu.cn*

[b]*Collaborative Innovation Center of Extreme Optics, Shanxi University, Taiyuan, Shanxi 030006, China*

[c]*Department of Optical Science and Engineering, Fudan University, Shanghai 200433, China. E-mail: qyjin@fudan.edu.cn*

imidazolate linkers (*e.g.* 2-methylimidazole).[28] The connectivity of the M–IM–M units results in large pore size and volume, which therefore points toward their potential usage as sorption materials.[29,30] The compound is characterized by a sodalite zeolite-type structure and featuring large cavities (11.6 Å) and small apertures (3.4 Å), it is well known for its chemical robustness and thermal stability,[31,32] which is assumed to play a role in sensing studies. Since the discovery of the first ZIFs sample, previous studies have been mostly focused on synthesizing new ZIFs and investigating their applications in gas storage[33] and detection,[34] separation ability,[35–37] and mainly using the Raman spectrum to detect molecules. Chen *et al.* encapsulated the oxygen sensing pyrene molecules within the pores of a $Zn(mim)_2$ framework (ZIF-8, mim = 2-methylimidazolate).[37] Li *et al.* chose ZIF-8 to fabricate a hollow MOF nanoshell-based etalon (HMNSE), to yield selective volatile organic compounds (VOCs) with distinctive colour output and top-notch efficiency of optical transduction.[38,39] However, the preliminary work primarily regarded ZIF-8 as the container of the guest molecule, and there are few studies that focus on ZIF-8 fluorescence emission and regard ZIF-8 as a host.

In this work, we aim to explore the photoluminescence emission of ZIF-8 with other fluorescent molecules, based on the following considerations: (1) ZIF-8 can be easily synthesized in organic solvent at room temperature, which allows a broader selection of dyes;[40,41] (2) the emission peak of ZIF-8 is located in the visible light range which easy to find the fluorescence matching molecules. Using 2-(2-hydroxyphenyl)-1*H*-benzimidazole (HPBI) as an analyte, with a high-efficiency fluorescence yield, has applications in the fields of biological probes and fluorescent dyes.

2 Methods

2.1 Synthesis of ZIF-8

Zinc nitrate hexahydrate ($N_2O_6Zn\cdot 6H_2O$, 99%) and 2-methylimidazole ($C_4H_6N_2$, 98%) were commercially available and used without further purification. On the basis of zinc salt and 2-methylimidazole in a molar ratio of 1 : 1, we tried to mix 5 mL solution of 2-methylimidazole (25 mM, in MeOH) and 5 mL solution of $N_2O_6Zn\cdot 6H_2O$ (25 mM, in MeOH).[42–44] The solutions were then allowed to react at room temperature for 24 hours without stirring. The product was collected by centrifugation, washed three times with methanol, and then preserved with ethanol as the solvent for later photoluminescence experiments.[45]

HPBI solution preparation. 2-(2-Hydroxyphenyl)-1*H*-benzimidazole (HPBI, 95%) was purchased from Aladdin company. 18.8 mg of HPBI was immersed in 17.885 mL ethanol, and the suspension was used for luminescent measurements. Here the concentration of HPBI was 5×10^{-3} mol L^{-1} as the stock solution was prepared and then diluted to the desired concentrations with ethanol.

2.2 HPBI with ZIF-8 mixture preparation

We diluted the stock solution to receive five gradient solutions: 1×10^{-5} mol L^{-1}, 1×10^{-4} mol L^{-1}, 2×10^{-4} mol L^{-1}, 5×10^{-4} mol L^{-1} and 1×10^{-3} mol L^{-1}. We added 100 μl ZIF-8 solvent into 1 mL of five different concentrations of HPBI separately, mixing well under ultrasonic conditions, and the hybrid solution was then prepared for the photoluminescence experiments.

2.3 Sample characterization

All the luminescence emission spectra of the samples were obtained with a liquid nitrogen cooled charge coupled device (CCD) spectrometer (Princeton Instruments) *via* an optical fiber. The fluorescence lifetime was obtained by an optical fiber connected to a microchannel plate photomultiplier tube (Hamamatsu) combined with time-correlated single photon counting technique (TCSPC, Edinburgh Instruments). A pulse picosecond semiconductor laser at 375 nm (Advance Laser System) was used to excite the samples. The scanning electron microscope (Zeiss Gemini 450) and the transmission electron microscope (JEM-2100F) were used to examine crystal morphology. XRD spectra were collected using Ultima IV. The distribution and dimension of HPBI molecules on the substrates was characterized by scanning tunneling microscope (STM, CREATEC). The N_2 adsorption/desorption isotherms and surface area were obtained using a Micromeritics ASAP2020 analyzer. X-ray photoelectron spectra were collected on an XPS-Nexsa (Thermo Fisher Scientific).

3 Results and discussion

ZIF-8 was synthesized with methanolic solutions of zinc nitrate and 2-methylimidazole mixed together. As shown in Fig. 1a, ZIF-8 exhibits a sod topology formed by four- and six-membered ring $ZnNO_3$ clusters with internal cavities (yellow ball). Scanning electron microscope (SEM) images showed that the dispersed ZIF-8 nanoparticles were uniform hexagonal nanostructures with mean sizes around 880 nm (Fig. 1b). The X-ray powder diffraction (XRD) pattern in Fig. 1c demonstrated the crystallinity of synthesized ZIF-8. The peaks are in agreement with the typical structure of ZIF-8 reported previously.[29] As depicted in Fig. 1d, ZIF-8 exhibited a weak emission band at 450 nm under 375 nm laser excitation. It is known that MOFs with transition metal ions and those without unpaired electrons, especially those that have d^{10} configurations, can yield linker-based highly emissive materials. The luminescent behaviour of ZIF-8 was consistent with the previous results that the emission is in the region of the free ligand 2-methylimidazole.[12] The fact of a redshift (emission at 425 nm for 2-methylimidazole shifts to 450 nm for ZIF-8) with respect to the free ligand was probably caused by the coordination effect of 2-methylimidazole onto the Zn^{2+}.[12]

The structure of HPBI is shown in Fig. 2a. HPBI powder was evaporated and deposited on the Au(111) surface under ultra-high vacuum, capitalizing upon surface-assisted molecular self-assembly, a representative STM topograph at ~80 K is shown in Fig. 2b. At low coverage in the submonolayer regime, these chains were found to be tightly packed. The bunches of chains observed on Au(111) were typically straight and aligned parallel,

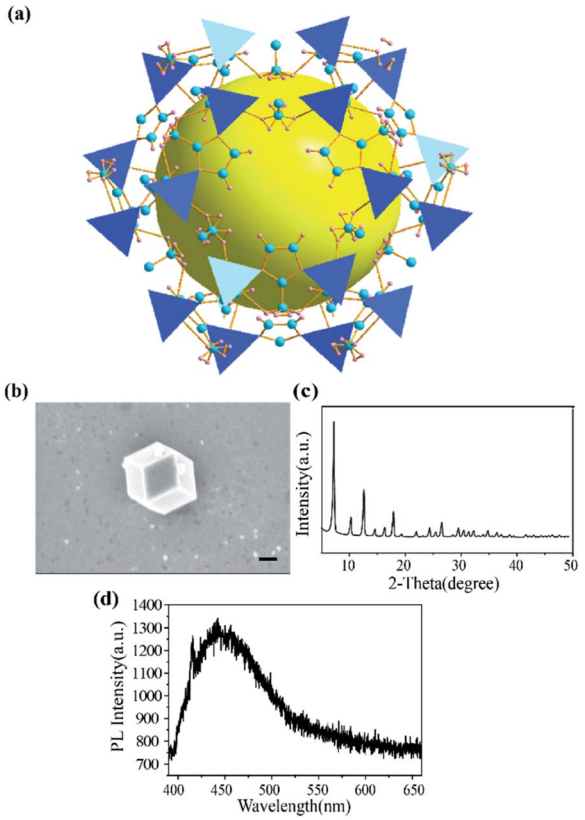

Fig. 1 (a) Crystal structure of ZIF-8: Zn (polyhedral), C (blue sphere), and H (pink sphere). The largest sphere (yellow) represents the largest van der Waals spheres that would fit in the cavities without touching the framework. (b) TEM images of ZIF-8 (scale bar: 300 nm). (c) XRD pattern of synthesized ZIF-8. (d) Fluorescence spectra of ZIF-8 under excitation at 375 nm.

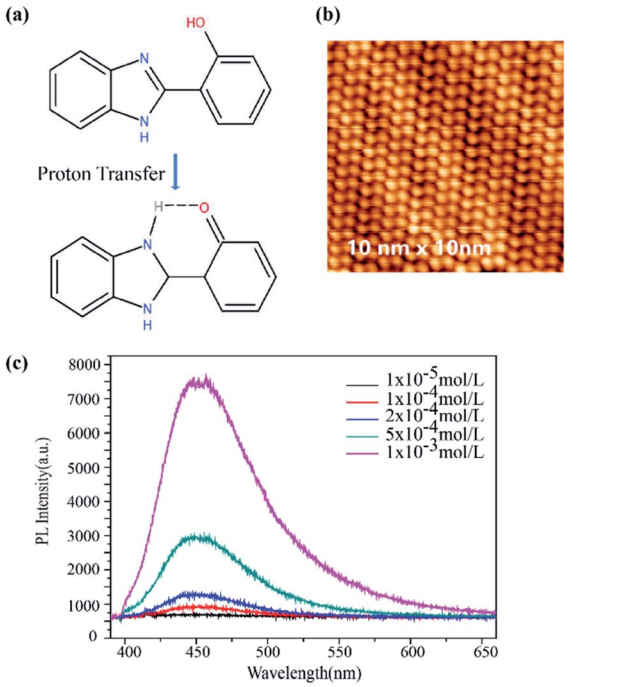

Fig. 2 (a) Chemical structure of HPBI and proton transfer of HPBI. (b) Typical STM image of HPBI on Au (111) (10 × 10 nm^2, −2.7 V, 10 pA). (c) Fluorescence spectra of HPBI with different concentrations under excitation at 375 nm.

and condensed into a monolayer wherein they remained intact, straight, and stacked together neatly. There is hydrogen bonding within each chain, whereas the attractive interaction between the chains is likely due to van der Waals forces.[46] With the STM image and HPBI chemical structure, the size of HPBI is around 3 × 7 Å.

The PL spectra of HPBI with different concentrations (1 × 10^{-6} mol L^{-1}, 1 × 10^{-5} mol L^{-1}, 1 × 10^{-4} mol L^{-1}, 2 × 10^{-4} mol L^{-1}, 5 × 10^{-4} mol L^{-1} and 1 × 10^{-3} mol L^{-1}) were plotted in Fig. 2c, exhibiting typical peaks at 450 nm. Benzimidazole molecules have a unique π–π* conjugated structure. When the carbon in the nitrogen heterocycle is connected to the 2-hydroxyphenyl group, it has a distinct fluorescence emission. HPBI and its derivatives are a series of important fluorescent compounds, these compounds have generated a lot of interest because of their intense emission properties *via* excited-state intramolecular proton transfer (ESIPT).[47,48] When the ESIPT effect occurs, the H proton on the hydroxyl group is transferred to the nitrogen atom on the imidazole ring, and intramolecular hydrogen bonding occurs with the N on the imidazole ring. N⋯HO and C form a six-membered ring structure (Fig. 2a). The excited-state intramolecular proton transfer luminescence has the advantages of large Stoke's shift, high fluorescence quantum yield, good light stability, and high luminescent efficiency. At the same time, ESIPT molecules have properties such as bistable state and optical nonlinearity, and the process is reversible, which can also be used in optical switches and optical storage systems.[49] The degree of the conjugated system is greatly increased and the energy is reduced, with a long-wavelength emission peak (450 nm) appearing. The fluorescence emission peaks of HPBI and ZIF-8 were both around 450 nm, which facilitates resonance enhancement.[50]

The interaction between HPBI and ZIF-8 after mixing can be seen in the following scheme (Fig. 3a). When HPBI and ZIF-8 are combined, the HPBI may be adsorbed with the pore framework structure. The TEM images (Fig. 3b) revealed ZIF-8 mixed with HPBI molecules. The polyhedral shape of the ZIF-8 had no obvious changes, the morphology confirmed the structural stability, but the edge became more obscure. We suspected this was due to the aggregation of HPBI molecules adsorbed and accumulated on the outer surfaces of ZIF-8. Fig. 3c showed the corresponding EDS elemental mapping of ZIF-8 with HPBI mixture, the oxygen came from HPBI and we could see it distributed throughout the ZIF-8, which verified the speculation that HPBI molecules were distributed around the ZIF-8 framework pores. We compared the TEM images and mapping images of the ZIF-8 sample (Fig. 3d and e) which also could see the oxygen element in the mapping, however the profile of ZIF-8 was not clear as a mixture, the oxygen in ZIF-8 may have come from the ethanol solvent. We suspected these crystals in a different shape attributed to the aggregation of HPBI molecules adsorbed and accumulated on the outer surfaces of ZIF-8.

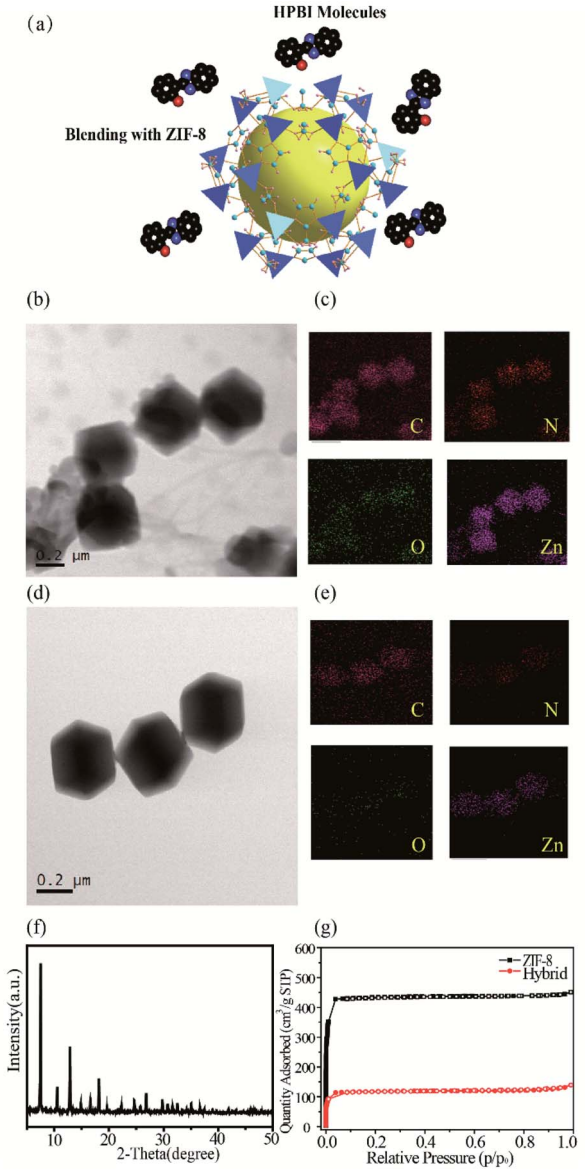

Fig. 3 (a) Scheme of HPBI molecules blending with ZIF-8; (b) TEM image of ZIF-8 with HPBI and (c) EDS elemental mapping of ZIF-8 nanoparticles after adding HPBI molecules; (d) TEM image of ZIF-8 and (e) EDS elemental mapping of ZIF-8 nanoparticles; (f) XRD pattern of synthesized ZIF-8 and HPBI hybrid; (g) N_2 sorption isotherms of ZIF-8 nanoparticles at 77 K before and after HPBI adsorption. Solid symbols (square and circle) correspond to adsorption plots and open symbols correspond to desorption plots.

The X-ray powder diffraction (XRD) pattern in Fig. 3f demonstrated the crystallinity of the hybrid and we compared it with the ZIF-8 pattern, which has no change in the crystallinity. We described ZIF-8 + HPBI as hybrid in Fig. 3–7.

The gas sorption behavior and surface area of nanosized ZIF-8 were determined by the N_2 sorption isotherm at 77 K (Fig. 3g). The gravimetric Brunauer–Emmett–Teller (BET) surface area of the synthesized ZIF-8 was found to be 1892 $m^2\ g^{-1}$, which is consistent with those previously reported for nanoscale ZIF-8.[51] As HBPI was mixed with ZIF-8, the BET surface area decreased to 515 $m^2\ g^{-1}$, which illustrated that HPBI molecules were captured by ZIF-8.

Further investigations of HPBI and ZIF-8 surface interactions were performed using X-ray photoelectron spectroscopy (XPS). Typical peaks representative of ZIF-8 were present (Fig. 4). The broad peak in the C (1 s) spectrum is attributed to the C=N/C=C, C–H/C–C peaks. The broad N (1s) peak is ascribed to the convolution of three different species (N–Zn/N–H, N–C, N=C).[29] The two peaks in the Zn (2p) spectrum are assigned to Zn $2p_{3/2}$ and Zn $2p_{1/2}$.[52] The surface chemistry of bound species probed by XPS shows distinct features that arise due to HPBI adsorption. In the O (1s), an obvious intensity enhancement is observed after HPBI adsorption. The N (1s) peak at 398.98 eV corresponds to 2-methylimidazole in ZIF-8 based on a comparison to previously reported values for bulk ZIF-8.[51] A 60.9% decrease in the intensity of the N (1s) spectrum shown after HPBI adsorption suggested the direct involvement of nitrogen functionalities of the imidazolate linker. Furthermore, the C (1 s) shows notable changes upon mixing with HPBI.

The luminescent measurements of the hybrid solution were conducted under the same conditions and carried out at room temperature. The fluorescence spectra were collected after ultrasonic blending. After adding ZIF-8 into HPBI solution (1×10^{-4} mol L^{-1}), with the increase in mixing time, HPBI wrapped well on the surface of ZIF-8 and the fluorescence intensity increased, then the fluorescence intensity enhancement stopped with the coverage saturated. It is noteworthy that the PL for HPBI and ZIF-8 hybrid solution (Fig. 5a) displayed a significantly enhanced and blue shift from 450 nm to 410 nm compared to that of HPBI, all of which indicates that the pore of

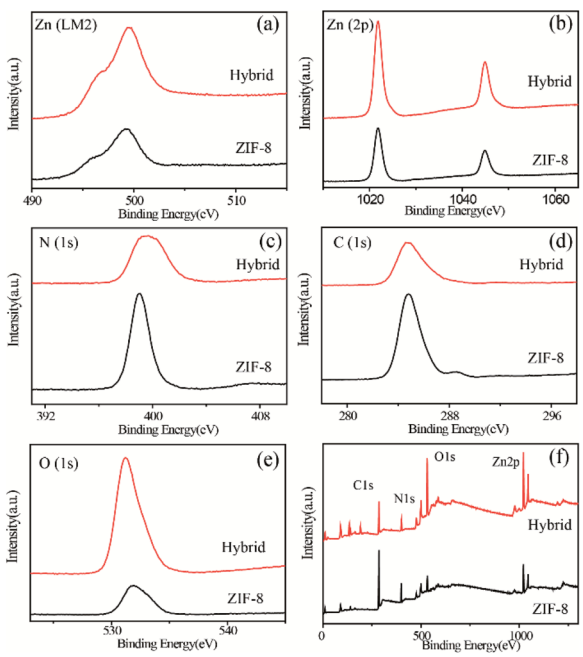

Fig. 4 XPS spectra of pristine ZIF-8 (black) and ZIF-8 and HPBI hybrid (red) at the (a) Zn (LM2), (b) Zn (2p), (c) N (1 s), (d) C (1 s), (e) O (1 s) and (f) whole elements.

ZIF-8 could restrict the molecular vibration and rotation, then lead to an enhanced emission efficiency.[53]

We measured the fluorescent response of different concentrations of HPBI in the presence of ZIF-8. The fluorescence spectra were collected after blending with ultrasonic treatment. As demonstrated in Fig. 5b, the emission intensity increased significantly with the increase of HPBI concentration from 1×10^{-5} mol L^{-1} to 2×10^{-4} mol L^{-1}. It was obvious to see that compared with the fluorescence intensity of HPBI (1×10^{-4} mol L^{-1}) alone, the fluorescence intensity of the hybrid was significantly enhanced (Fig. 5c), for the concentrations in 1×10^{-5} mol L^{-1} and 2×10^{-4} mol L^{-1} were similar to 1×10^{-4} mol L^{-1}. When the concentration increased to 5×10^{-4} mol L^{-1}, the emission intensity decreased, and then as we increased the concentration to 1×10^{-3} mol L^{-1}, the intensity of the hybrid was close to that of pure HPBI, which means that when the concentration of HPBI reached 1×10^{-3} mol L^{-1}, ZIF-8 had little enhancement effect. From Fig. 5d, we also found that when the emission intensity decreased, the location of the peak redshift compared with the maximum intensity peak location, and when the intensity of the hybrid was close to the PL intensity of the original HPBI, the peak of the hybrid liquid moved close to 450 nm (the tendency of 1×10^{-3} mol L^{-1} is similar to 5×10^{-3} mol L^{-1}). The hydrogen bonds formed by HPBI worsened the aggregation in the high concentration solution, which induced the emission to shift red.[54]

Additionally, for the further exploration of the role of Zn^{2+}, we mixed $Zn(NO_3)_2$ and HPBI to obtain the PL emission (Fig. 5e). The emission peak of the mixture had a blue shift when compared with pure HPBI, and the intensity was 1.5 times higher than pure HPBI. Based on the results from the emission spectrum, the blue shift may have occurred due to Zn^{2+}, but the framework structure of ZIF-8 resulted in the fluorescence enhancement of HPBI.

Fig. 5f show $\Delta I = I_{ZIF-8 + HPBI}/I_{HPBI}$ of ZIF-8 mixed with HPBI in five different concentrations, exhibiting the hybrid having the highest emission intensity at 1×10^{-4} mol L^{-1}, from the luminescent enhancement ΔI (Table 1), we can see that the maximum enhancement factor of 66 can be obtained and the mechanism for the fluorescence enhancement may be attributed to ZIF-8 particles with highly permanent pores providing a natural space to accommodate the guest molecules, increasing the chance of guest–host interaction and contributing to the sensitive detection of HPBI. The length of the HPBI molecules is around 3 Å and the width is around 7 Å (Fig. 2b), which even though is slightly larger than the aperture size (about 3.4 Å) of ZIF-8, with the flexible structure of ZIF-8, there are chances for HPBI molecules being absorbed by the ZIF-8 shell apertures.[55] The enhancement in fluorescence intensity due to the above mechanism is associated with the adsorption of the probe molecule and includes either molecule–metal or metal–molecule charge transfer. The above results revealed that the MOF sorption properties offer a high degree of molecular

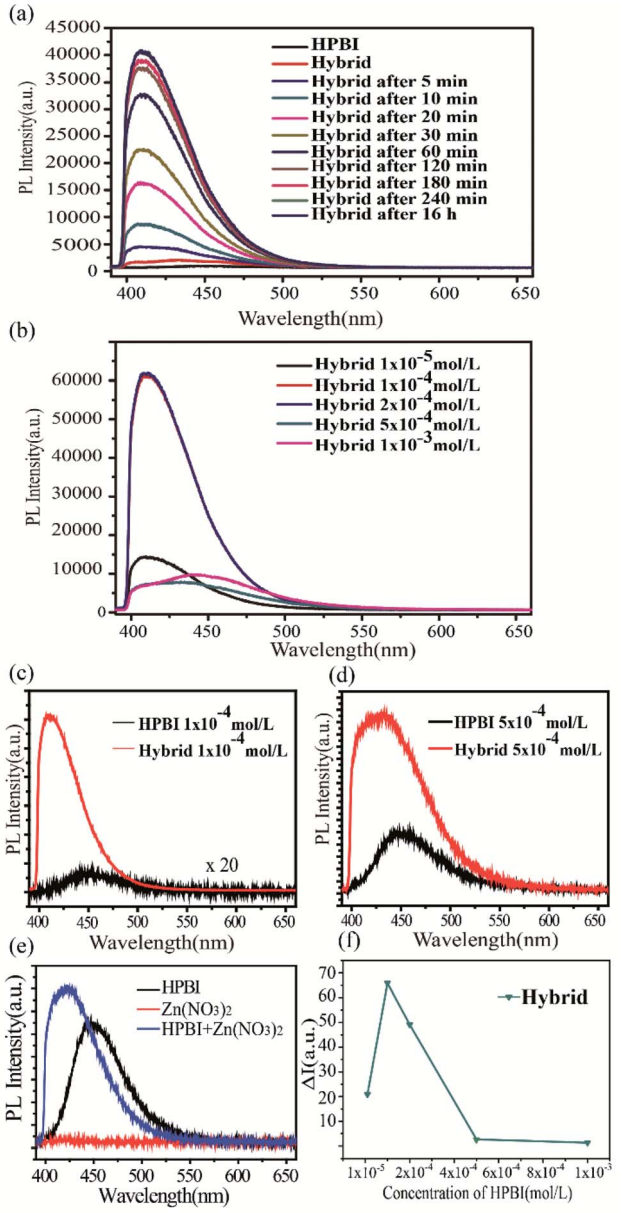

Fig. 5 (a) Fluorescence spectra of ZIF-8 with immersion time increased in the presence of HPBI (1×10^{-4} mol L^{-1}). (b) Fluorescence spectra of ZIF-8 in the presence of various concentrations of HPBI under excitation at 375 nm. (c) and (d) Comparing fluorescence spectra of HPBI and ZIF-8 (hybrid) with corresponding concentrations of HPBI (1×10^{-4} mol L^{-1} and 5×10^{-4} mol L^{-1}), the intensity of HPBI (1×10^{-4} mol L^{-1}) multiply by 20 in order to see the peak position (black line). (e) Comparing fluorescence spectra of HPBI and HPBI + $Zn(NO_3)_2$. (f) ΔI denotes the enhanced fluorescence intensity of HPBI with different concentrations after adding ZIF-8.

Table 1 ΔI of ZIF-8 with different concentration of HPBI

HPBI concentration (mol L^{-1})	ΔI
1×10^{-5}	20.88
1×10^{-4}	65.85
2×10^{-4}	49.14
5×10^{-4}	2.66
1×10^{-3}	1.33

detection. The adsorption mechanism of HPBI with ZIF-8 may be due to the strong π–π stacking interaction between aromatic rings, the imidazole ring of the skeleton of ZIF-8 and the benzene ring of HPBI seems likely to pass through π–π stacking interaction.[56,57] This phenomenon can be used for further exploration of the tiny fluorescence molecules sensing in different areas, and it is expected to further improve the accuracy of molecular sensing with aperture matching.

The fluorescence decay curves of different concentrations of HPBI with ZIF-8 as shown in Fig. 6a–e. Here are the similar trends in the lifetime, the curve of HPBI mixed with ZIF-8 (red) located between the ZIF-8 lifetime curve (black) and the HPBI lifetime curve (blue). When the concentration was below 2×10^{-4} mol L^{-1}, the lifetime of the mixture was closer to the ZIF-8 lifetime, and as HPBI concentration increased, the blend lifetime also increased, which got closer to the pure HPBI solution. However, the presence of Zn^{2+} in ZIF-8 limited the ESIPT process in HPBI to a certain extent. In addition to the limitation of rotation by the aperture of ZIF-8, the luminescence is mainly derived from the $\pi-\pi^*$ transition, at which time the blue shift of the fluorescence peak position occurs and the fluorescence lifetime of the molecule was reduced compared to that of the pure HPBI molecule.

Detailed lifetimes are listed in Table 2. Emission lifetimes (τ) were determined by fitting the decays to a single exponential and double exponential function: $I(t) = \alpha_1 e^{-t/\tau 1} + \alpha_2 e^{-t/\tau 2}$, where α is the pre-exponential factor, and t is the time.[58] HPBI was best fit to bi-exponentials, where the presence of more than one decay process with characteristic lifetime results in curvature of these spectra: the faster component has $\tau_1 = 0.76$–2.76 ns, the relative contribution of the longer-lived species, with a lifetime of 3.98–5.44 ns. Growth of a decay component with a longer lifetime at lower emission energy, along with a delay in emission, is indicative of an excited-state process (*i.e.*, the population of the long-lived emissive state occurs after initial excitation), presumably facilitated by interactions between individual molecules in HPBI.[59] In contrast, emission decays for ZIF-8 with HPBI mixture were best fitted by a mono-exponential function with $\tau 1 = 1.75$–1.94 ns, as the HPBI concentration increased, the lifetime can be well fitted by a bi-exponential function with $\tau 1 = 1.28$–1.55 ns and $\tau 2 = 2.90$–3.63 ns, this lifetime is shorter than that of pure HPBI molecules and the emission wavelength at 450 nm comes from ESIPT with highly rigidified shown previously,[60] indicating that the structure of HPBI in the mixture is not completely rigid now, and thus nonradiative decay pathways are not fully suppressed.

The possible fluorescence enhancement could be attributed to HPBI adsorbed by ZIF-8. The terminology of the HOMO–LUMO gap can be utilized to describe the luminescence of ZIF-8.[61,62] Electrons transfer from the highest occupied molecular orbital (HOMO) to the lowest unoccupied molecular orbital (LUMO) in ZIF-8 when given a certain amount of energy. Upon excitation by 375 nm laser, the electrons which are easier to trigger in HPBI molecules may be transferred to ZIF-8, eventually leading to an enhancement in fluorescence.[63,64]

We found that as the concentration of HPBI increased, the aggregation of HPBI on the surface of ZIF-8 increased, which

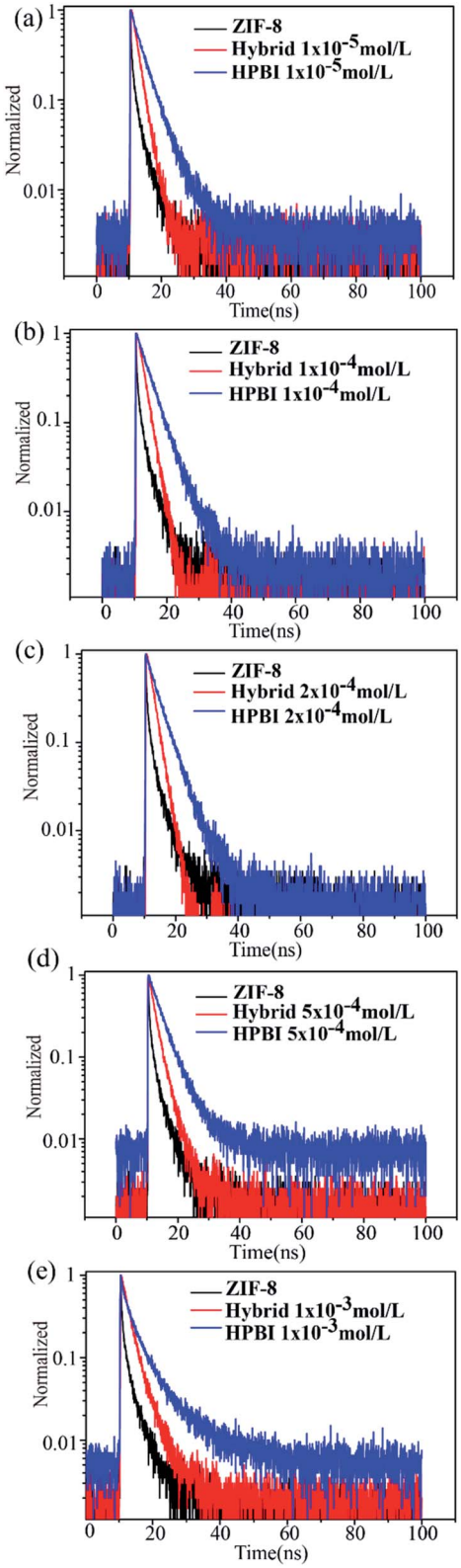

Fig. 6 Dynamics of PL decay of ZIF-8 with different concentrations of HPBI (a) 1×10^{-5} mol L^{-1}, (b) 1×10^{-4} mol L^{-1}, (c) 2×10^{-4} mol L^{-1}, (d) 5×10^{-4} mol L^{-1} and (e) 1×10^{-3} mol L^{-1}.

Table 2 Lifetime of ZIF-8 with different concentration of HPBI

	HPBI concentration (mol L^{-1})	Zeta-potential (mV)
ZIF-8	0	22.6
Hybrid	1×10^{-5}	16.6
	1×10^{-4}	−1.88
	2×10^{-4}	−30.5
	5×10^{-4}	−53.7
	1×10^{-3}	−48.8

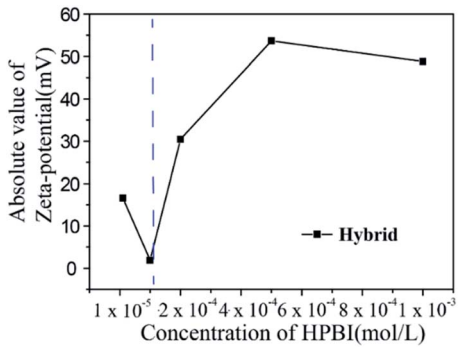

Fig. 7 Effect of HPBI concentration on the zeta-potential.

can be shown with the enhancement of fluorescence intensity, so we used zeta-potential for further research of the aggregation of HPBI. Zeta-potential analysis is a technique for determining the dispersion stability of nanoparticles in solution.

Zeta-potential analyses are often used to improve the formulation of dispersions, emulsions, and suspensions.[65] The zeta-potential of different concentrations of HPBI blending with ZIF-8 in Table 3, when ZIF-8 hybrid with HPBI, the zeta-potential of the hybrid solution decreased compared with the pure ZIF-8, this can be attributed to the effect of HPBI adsorption on the surface of ZIF-8, which decreases the zeta-potential of ZIF-8 and thus reduces the charge. It can be seen from Fig. 7 and Table 3 that the absolute value at 1×10^{-4} mol L^{-1} is smaller than the other concentrations and pure ZIF-8 zeta-potential, which suggested instability under these conditions. We can assume that HPBI molecules were adsorbed by ZIF-8 at the saturated concentration 1×10^{-4} mol L^{-1}, which corresponds with the enhanced fluorescence intensity results (Fig. 5f).

Table 3 Zeta-potential of ZIF-8 with different concentration of HPBI

	HPBI concentration (mol L^{-1})	τ_1 (ns), A_1	τ_2 (ns), A_2	τ_3 (ns), A_3
ZIF-8	0	0.03, 22	0.77, 34	3.64, 44
Pure HPBI	1×10^{-5}	0.76, 10	3.98, 90	
	1×10^{-4}	0.61, 6	3.98,94	
	2×10^{-4}	2.70, 50	3.99, 92	
	5×10^{-4}	2.76, 49	5.44, 51	
	1×10^{-3}	1.35, 30	6.01, 70	
Hybrid	1×10^{-5}	1.75		
	1×10^{-4}	1.75		
	2×10^{-4}	1.94		
	5×10^{-4}	1.28, 40	2.90, 60	
	1×10^{-3}	1.55, 52	3.63, 48	

4 Conclusions

In summary, we explored the ability of ZIF-8 to sense and tune luminescent small molecules HPBI when the guest molecules and host fluorescence emission peaks are located in the same range. Faster adsorption of HPBI molecules over ZIF-8 was observed in photoluminescence spectra and lifetime. Photo-induced emission intensity enhancement due to guest adsorption with peak shift as the concentration increased. As the concentration increased to 5×10^{-4} mol L^{-1}, the luminescent enhancement effect of ZIF-8 decreased, the ΔI was even near 1 which means the intensity near the pure HPBI fluorescence intensity, and the ability of adsorption saturated. In addition to the intensity change, the PL peak also shifted from 450 nm to 410 nm as the PL intensity increased. The blue shift could be ascribed to the ESIPT of such organic compounds, with the molecular vibration and rotation restricted by ZIF-8. Furthermore, energy shifting can also be confirmed by lifetime. The adsorption process was investigated *via* the measurements of zeta-potentials, which further demonstrated the adsorption process of HPBI by the porous structure of ZIF-8 and the adsorption with a saturation concentration. The experimental results for emission spectra, lifetime decay and zeta-potential are self-consistent. For further research, one can use ZIF-8 in sensing nanoscale molecules *via* luminescence enhancement, which receives fluorescence responses more quickly. This work will further expand the application of ZIF-8 in the field of fluorescent molecular sensing.

Author contributions

X. Z., M. C., B. H. and Q. J. supervised the project, designed experiments, and analysed the data. Y. Z., W. Z., Y. B. and Y. L. performed experiments and analysed data. Y. Z., X. Z. and M. C. wrote the paper. B. H. and Q. J. edited the paper.

Conflicts of interest

There are no conflicts to declare.

Acknowledgements

This work was supported by the National Key R&D Program of China (2017YFA0303403), the National Natural Science Foundation of China (Grant No. 11874015, 21802043) and Program of Introducing Talents of Discipline to Universities (B12024).

References

1 U. P. N. Tran, K. K. A. Le and N. T. S. Phan, *ACS Catal.*, 2011, **1**, 120–127.

2 Y. He, B. Li, M. O'Keeffe and B. Chen, *Chem. Soc. Rev.*, 2014, **43**, 5618–5656.
3 J. L. C. Rowsell and O. M. Yaghi, *Microporous Mesoporous Mater.*, 2004, **73**, 3–14.
4 Y. B. Hao, Z. S. Shao, C. Cheng, X. Y. Xie, J. Zhang, W. J. Song and H. S. Wang, *ACS Appl. Mater. Interfaces*, 2019, **11**, 31755–31762.
5 S. Furukawa, J. Reboul, S. Diring, K. Sumida and S. Kitagawa, *Chem. Soc. Rev.*, 2014, **43**, 5700–5734.
6 A. Betard and R. A. Fischer, *Chem. Rev.*, 2012, **112**, 1055–1083.
7 H. Li, K. Wang, Y. Sun, C. T. Lollar, J. Li and H.-C. Zhou, *Mater. Today*, 2018, **21**, 108–121.
8 Y. P. Xue, G. C. Zhao, R. Y. Yang, F. Chu, J. Chen, L. Wang and X. B. Huang, *Nanoscale*, 2021, **13**, 3911–3936.
9 W. Q. Zhou, B. H. Zou, W. N. Zhang, D. B. Tian, W. Huang and F. W. Huo, *Nanoscale*, 2015, **7**, 8720–8724.
10 L. Esrafili, A. Morsali, M. L. Hu, A. Azhdari Tehrani, L. Carlucci, P. Mercandelli and D. M. Proserpio, *Inorg. Chem.*, 2020, **59**, 16421–16429.
11 W. Yao, J. Wang, A. Zhong, J. Li and J. Yang, *Org. Lett.*, 2020, **22**, 8086–8090.
12 S. Liu, Z. Xiang, Z. Hu, X. Zheng and D. Cao, *J. Mater. Chem.*, 2011, **21**, 6649–6653.
13 D. J. Cram, S. Karbach, H. E. Kim, C. B. Knobler, E. F. Maverick, J. L. Ericson and R. C. Helgeson, *J. Am. Chem. Soc.*, 2002, **110**, 2229–2237.
14 S. Das and P. K. Bharadwaj, *Inorg. Chem.*, 2006, **45**, 5257–5259.
15 O. Abuzalat, D. Wong, S. S. Park and S. Kim, *Nanoscale*, 2020, **12**, 13523–13530.
16 M.-L. Hu, S. A. A. Razavi, M. Piroozzadeh and A. Morsali, *Inorg. Chem. Front.*, 2020, **7**, 1598–1632.
17 Q. Yang, Y. Wen, A. Zhong, J. Xu and S. Shao, *New J. Chem.*, 2020, **44**, 16265–16268.
18 L. He, B. Dong, Y. Liu and W. Lin, *Chem. Soc. Rev.*, 2016, **45**, 6449–6461.
19 D. J. Wales, J. Grand, V. P. Ting, R. D. Burke, K. J. Edler, C. R. Bowen, S. Mintova and A. D. Burrows, *Chem. Soc. Rev.*, 2015, **44**, 4290–4321.
20 L. E. Kreno, K. Leong, O. K. Farha, M. Allendorf, R. P. Van Duyne and J. T. Hupp, *Chem. Rev.*, 2012, **112**, 1105–1125.
21 Y. W. Zhao, J. N. Wang, W. P. Zhu, L. F. Liu and R. J. Pei, *Nanoscale*, 2021, **13**, 4505–4511.
22 L. G. Qiu, Z. Q. Li, Y. Wu, W. Wang, T. Xu and X. Jiang, *Chem. Commun.*, 2008, 3642–3644.
23 X. Zou, G. Zhu, I. J. Hewitt, F. Sun and S. Qiu, *Dalton Trans.*, 2009, 3009–3013.
24 S. L. Zheng, J. P. Zhang, X. M. Chen, Z. L. Huang, Z. Y. Lin and W. T. Wong, *Chemistry*, 2003, **9**, 3888–3896.
25 M. D. Allendorf, C. A. Bauer, R. K. Bhakta and R. J. Houk, *Chem. Soc. Rev.*, 2009, **38**, 1330–1352.
26 Z.-Q. Li, L.-G. Qiu, W. Wang, T. Xu, Y. Wu and X. Jiang, *Inorg. Chem. Commun.*, 2008, **11**, 1375–1377.
27 A. Lan, K. Li, H. Wu, D. H. Olson, T. J. Emge, W. Ki, M. Hong and J. Li, *Angew. Chem., Int. Ed.*, 2009, **48**, 2334–2338.
28 S. Pramanik, C. Zheng, X. Zhang, T. J. Emge and J. Li, *J. Am. Chem. Soc.*, 2011, **133**, 4153–4155.
29 A. M. Ebrahim, A. M. Plonka, N. Rui, S. Hwang, W. O. Gordon, A. Balboa, S. D. Senanayake and A. I. Frenkel, *ACS Appl. Mater. Interfaces*, 2020, **12**, 58326–58338.
30 J. Perez-Pellitero, H. Amrouche, F. R. Siperstein, G. Pirngruber, C. Nieto-Draghi, G. Chaplais, A. Simon-Masseron, D. Bazer-Bachi, D. Peralta and N. Bats, *Chemistry*, 2010, **16**, 1560–1571.
31 K. S. Park, Z. Ni, A. P. Côté, J. Y. Choi, R. Huang, F. J. Uribe-Romo, H. K. Chae, M. O'Keeffe and O. M. Yaghi, *Proc. Natl. Acad. Sci. U. S. A.*, 2006, **103**, 10186–10191.
32 G. Lu, S. Li, Z. Guo, O. K. Farha, B. G. Hauser, X. Qi, Y. Wang, X. Wang, S. Han, X. Liu, J. S. DuChene, H. Zhang, Q. Zhang, X. Chen, J. Ma, S. C. Loo, W. D. Wei, Y. Yang, J. T. Hupp and F. Huo, *Nat. Chem.*, 2012, **4**, 310–316.
33 L. Mu, B. Liu, H. Liu, Y. Yang, C. Sun and G. Chen, *J. Mater. Chem.*, 2012, **22**, 12246–12252.
34 K. Huang, S. Gong, L. Zhang, H. Zhang, S. Li, G. Ye and F. Huang, *Chem. Commun.*, 2021, **57**, 2144–2147.
35 K. Zhang, R. P. Lively, C. Zhang, W. J. Koros and R. R. Chance, *J. Phys. Chem. C*, 2013, **117**, 7214–7225.
36 R. Kumar, K. Jayaramulu, T. K. Maji and C. N. Rao, *Chem. Commun.*, 2013, **49**, 4947–4949.
37 J. W. Ye, H. L. Zhou, S. Y. Liu, X. N. Cheng, R. B. Lin, X. L. Qj, J. P. Zhang and X. M. Chen, *Chem. Mater.*, 2015, **27**, 8255–8260.
38 W. P. Lustig, S. Mukherjee, N. D. Rudd, A. V. Desai, J. Li and S. K. Ghosh, *Chem. Soc. Rev.*, 2017, **46**, 3242–3285.
39 C. Li, L. Li, S. Yu, X. Jiao and D. Chen, *Adv. Mater. Technol.*, 2016, **1**, 1600127.
40 Y. Pan, D. Heryadi, F. Zhou, L. Zhao, G. Lestari, H. Su and Z. Lai, *CrystEngComm*, 2011, **13**, 6937–6940.
41 J. Zhuang, C. H. Kuo, L. Y. Chou, D. Y. Liu, E. Weerapana and C. K. Tsung, *ACS Nano*, 2014, **8**, 2812–2819.
42 J. Cravillon, R. Nayuk, S. Springer, A. Feldhoff, K. Huber and M. Wiebcke, *Chem. Mater.*, 2011, **23**, 2130–2141.
43 N. Yanai, M. Sindoro, J. Yan and S. Granick, *J. Am. Chem. Soc.*, 2013, **135**, 34–37.
44 W. Zhang, Y. Y. Zhang, Y. J. Bian, M. D. Chen, X. L. Zhang, Q. Y. Jin and B. W. Hu, *Chin. J. Inorg. Chem.*, 2021, **37**, 2059–2067.
45 S. Li, W. Zhang and F. Huo, *Phys. E*, 2015, **69**, 56–60.
46 P. S. Costa, D. P. Miller, J. D. Teeter, S. Beniwal, E. Zurek, A. Sinitskii, J. Hooper and A. Enders, *J. Phys. Chem. C*, 2016, **120**, 5804–5809.
47 H. Konoshima, S. Nagao, I. Kiyota, K. Amimoto, N. Yamamoto, M. Sekine, M. Nakata, K. Furukawa and H. Sekiya, *Phys. Chem. Chem. Phys.*, 2012, **14**, 16448–16457.
48 Y.-P. Tong, S.-L. Zheng and X.-M. Chen, *Eur. J. Inorg. Chem.*, 2005, **2005**, 3734–3741.
49 R. de Vivie-Riedle, V. De Waele, L. Kurtz and E. Riedle, *J. Phys. Chem. A*, 2003, **107**, 10591–10599.
50 M. M. Balamurali and S. K. Dogra, *Chem. Phys.*, 2004, **305**, 95–103.

51 M. Chin, C. Cisneros, S. M. Araiza, K. M. Vargas, K. M. Ishihara and F. Tian, *RSC Adv.*, 2018, **8**, 26987–26997.
52 Z. Liu, A. Wu, H. Yan, D. Su, C. Jin, H. Guo, L. Wang and C. Tian, *Chem. Commun.*, 2020, **56**, 2913–2916.
53 J. Mei, N. L. C. Leung, R. T. K. Kwok, J. W. Y. Lam and B. Z. Tang, *Chem. Rev.*, 2015, **115**, 11718–11940.
54 H. Xu, Z.-F. Xu, Z.-Y. Yue, P.-F. Yan, B. Wang, L.-W. Jia, G.-M. Li, W.-B. Sun and J.-W. Zhang, *J. Phys. Chem. C*, 2008, **112**, 15517–15525.
55 Q. Ding, J. Wang, X. Chen, H. Liu, Q. Li, Y. Wang and S. Yang, *Nano Lett.*, 2020, **20**, 7304–7312.
56 Y. Zhong, C. Chen, S. Liu, C. Lu, D. Liu, Y. Pan, H. Sakiyama, M. Muddassir and J. Liu, *Dalton Trans.*, 2021, **50**, 18016–18026.
57 C. Wu, Z. Xiong, C. Li and J. Zhang, *RSC Adv.*, 2015, **5**, 82127.
58 C. A. Bauer, T. V. Timofeeva, T. B. Settersten, B. D. Patterson, V. H. Liu, B. A. Simmons and M. D. Allendorf, *J. Am. Chem. Soc.*, 2007, **129**, 7136–7144.
59 G. Urbina-Villalba and M. García-Sucre, *Colloids Surf., A*, 2001, **190**, 111–116.
60 H. Konoshima, S. Nagao, I. Kiyota, K. Amimoto, N. Yamamoto, M. Sekine, M. Nakata, K. Furukawa and H. Sekiya, *Phys. Chem. Chem. Phys.*, 2012, **14**, 16448–16457.
61 H.-P. Jing, C.-C. Wang, Y.-W. Zhang, P. Wang and R. Li, *RSC Adv.*, 2014, **4**, 54454–54462.
62 M. A. Nasalevich, M. van der Veen, F. Kapteijn and J. Gascon, *CrystEngComm*, 2014, **16**, 4919–4926.
63 Q. Liu, S. Tian, X. Zhao and G. Sankar, *J. Mater. Chem. C*, 2021, **9**, 5819–5826.
64 J.-Q. Liu, Z.-D. Luo, Y. Pan, A. Kumar Singh, M. Trivedi and A. Kumar, *Coord. Chem. Rev.*, 2020, **406**, 213145.
65 M. Hesampour, A. Krzyzaniak and M. Nystrom, *J. Membr. Sci.*, 2008, **325**, 199–208.